Optical Constants of Sodium and Potassium from 0.5 to 4.0 eV by Split-Beam Ellipsometry*

NEVILLE V. SMITH†
Stanford Electronics Laboratory, Stanford University, Stanford, California 94305
(Received 25 March 1969)

The optical constants of sodium and potassium have been measured at room temperature over the frequency range 0.5–4.0 eV. The measurements were made with a split-beam ellipsometer, using a null procedure devised to yield the imaginary part of the dielectric constant, ϵ_2, with improved reliability. The samples were thick films prepared by evaporation in ultrahigh vacuum. Experiments were performed by single reflection at free surfaces, and by both single and multiple reflections at metal-fused quartz interfaces. All measurements were in agreement; however, the most accurate values for ϵ_2 were obtained in the multiple reflection experiments. They showed structure as a function of frequency which could be readily attributed to conventional interband transitions associated with the ⟨110⟩ reciprocal lattice vectors. The values obtained for ϵ_1 in both the free-surface and the metal-quartz-interface experiments were used to deduce the optical effective mass m_{opt}. For sodium, m_{opt} was found to be $1.13m$ in the infrared and $1.07m$ for wavelengths below $0.5\,\mu$; the corresponding values for potassium were found to be $1.16m$ and $1.06m$.

I. INTRODUCTION

SODIUM and potassium are regarded as good examples of nearly-free-electron behavior. However, because of the severe difficulties in obtaining clean surfaces of these reactive materials, very little optical work has been done on them. Early measurements were made by Ives and Briggs[1,2] and by Duncan and Duncan,[3] and the former have been analyzed in terms of nearly free-electron theory by Butcher[4] and by Cohen.[5] More recently, measurements have been extended into the infrared by Hodgson,[6,7] by Mayer and co-workers,[8,9] and by Althoff and Hertz,[10] and into the vacuum ultraviolet by Sutherland and co-workers.[11,12] The most extensive work was by Mayer *et al.*, and their results for the optical absorption, at photon energies below the interband threshold, revealed unexpected peaks which have stimulated considerable theoretical interest.[13–21] Several authors have suggested that many-body effects are more important in optical absorption than has been recognized. So it was with a view to learning something about many-body effects that the present experimental project was initiated.

It was decided, first of all, to make independent measurements of the optical constants; and the preliminary results have already been published.[22] No evidence has been found for the anomalous peaks. Our results are in good agreement, at least qualitatively, with the predictions of the nearly free-electron model. In this paper, we describe in greater detail how these experiments were performed, and present more extensive results and interpretation. Concurrently with the optical experiments, measurements were also made of the photoemission properties of Na and K. This work, however, is reported in a separate paper.[23]

The ellipsometric method was chosen for this work because of its great sensitivity. It was obvious in the design stages that, due to the extremely small absorption of the alkali metals, even this method would be pushed to the limits of its reliability. The problem arises from the fact that the ratio r_p/r_s of the two principal reflectivities is very close to unity for Na and K. The values obtained in this work, for example, were all greater than about 0.98. The absorption is proportional to the difference $1-r_p/r_s$, and so we are involved at the outset in the dubious procedure of subtracting two nearly equal quantities. An ellipsometer has been built based on a differential principle, and in Sec. II, we describe a null procedure which was devised, and which goes some way towards overcoming this problem. A more substantial improvement in accuracy was obtained by means of a multiple reflection technique, the cumulative effect of several reflections being simply to boost the total absorption.

* Work supported by Advanced Research Projects Agency through the Center for Materials Research at Stanford University.

† Present address: Bell Telephone Laboratories, Murray Hill, N. J. 07974.

[1] H. E. Ives and H. B. Briggs, J. Opt. Soc. Am. **26**, 238 (1936).
[2] H. E. Ives and H. B. Briggs, J. Opt. Soc. Am. **27**, 181 (1937).
[3] R. W. Duncan and R. C. Duncan, Phys. Rev. **1**, 294 (1913).
[4] P. N. Butcher, Proc. Phys. Soc. (London) **A64**, 50 (1951).
[5] M. H. Cohen, Phil. Mag. **3**, 762 (1958).
[6] J. N. Hodgson, J. Phys. Chem. Solids **24**, 1213 (1963).
[7] J. N. Hodgson, Phys. Letters **7**, 300 (1963).
[8] H. Mayer and M. H. el Naby, Z. Physik **174**, 289 (1963).
[9] H. Mayer and B. Hietel, in *Proceedings of the International Colloquium on Optical Properties and Electronic Structure of Metals and Alloys, Paris, 1965*, edited by F. Abeles (North-Holland Publishing Co., Amsterdam, 1966), p. 47.
[10] R. Althoff and J. H. Hertz, Infrared Phys. **7**, 11 (1967).
[11] J. C. Sutherland, E. T. Arakawa, and R. N. Hamm, J. Opt. Soc. Am. **57**, 645 (1967).
[12] J. C. Sutherland and E. T. Arakawa, J. Opt. Soc. Am. **58**, 1080 (1968).
[13] M. H. Cohen and J. C. Phillips, Phys. Rev. Letters **12**, 662 (1964).
[14] M. H. Cohen, Phys. Rev. Letters **12**, 664 (1964).
[15] A. W. Overhauser, Phys. Rev. Letters **13**, 196 (1965).
[16] M. H. Cohen, Ref. 9, p. 66.
[17] R. A. Ferrel, Ref. 9, p. 78.
[18] S. Nettel, Phys. Rev. **150**, 421 (1966).
[19] N. V. Smith, Phys. Rev. **163**, 552 (1967).
[20] K. L. Kliewer and R. Fuchs, Phys. Rev. **172**, 607 (1968).
[21] E-Ni. Foo and J. J. Hopfield, Phys. Rev. **173**, 635 (1968).
[22] N. V. Smith, Phys. Rev. Letters **21**, 96 (1968).
[23] N. V. Smith and W. E. Spicer (to be published).

In Sec. III, the results for the optical constants at room temperature are presented and compared with the predictions of the nearly free-electron model. The agreement is good insofar as we observe structure in the absorption, whose threshold corresponds very well to where we would expect the onset of conventional interband transitions. A complete analysis, however, is hampered by the observation of a rather large Drude background whose origin is not yet fully understood. The results for ϵ_1, the real part of the dielectric constant, are also presented in Sec. III, and are used to deduce values for the optical mass and the plasma frequency. An attempt is made to reconcile the behavior of ϵ_1 at the shorter wavelengths with interband transitions observed in the optical absorption. This is not entirely successful, and suggests the possible existence of further structure in the absorption at even shorter wavelengths.

II. EXPERIMENTAL METHOD

A. General Considerations

In the ellipsometric method, the procedure is to shine linearly polarized light onto the surface of the sample at some large angle of incidence φ. The electric vector of the incident light may be resolved into components parallel and perpendicular to the plane of incidence called, respectively, the p and s components and having different amplitude reflectivities $r_p e^{i\Delta_p}$ and $r_s e^{i\Delta_s}$. The quantity actually measured is the ratio

$$\tan\psi e^{i\Delta}=(r_p/r_s)e^{i(\Delta_p-\Delta_s)} \tag{1}$$

conventionally expressed in terms of a restored azimuth ψ and a differential phase change Δ. An analysis of the elliptically polarized reflected light yields values for ψ and Δ, which in turn yield values for ϵ_1 and ϵ_2, the real and imaginary parts of the dielectric constant, by substitution into the standard formulas[24]

$$\epsilon_1=\frac{\cos^2 2\psi-\sin^2 2\psi\,\sin^2\Delta}{(1+\cos\Delta\,\sin 2\psi)^2}\sin^2\varphi\,\tan^2\varphi+\sin^2\varphi, \tag{2}$$

$$\epsilon_2=\frac{2\,\sin 2\psi\,\cos 2\psi\,\sin\Delta}{(1+\cos\Delta\,\sin 2\psi)^2}\sin^2\varphi\,\tan^2\varphi. \tag{3}$$

For the alkali metals, it turns out that r_p/r_s is very close to unity and therefore ψ is very close to 45°. It is convenient to define a small angle β,

$$\beta=\tfrac{1}{4}\pi-\psi. \tag{4}$$

Since β is typically only a few tenths of a degree, Eqs. (2) and (3) reduce to

$$\epsilon_1\simeq-[\sin^2\Delta/(1+\cos\Delta)^2]\sin^2\varphi\,\tan^2\varphi+\sin^2\varphi, \tag{5}$$

$$\epsilon_2\simeq\beta[4\,\sin\Delta/(1+\cos\Delta)^2]\sin^2\varphi\,\tan^2\varphi. \tag{6}$$

First, we note that ϵ_2 is directly proportional to the small quantity β. On the other hand, ϵ_1 is independent of β and is determined by Δ. Moreover, we may expect ϵ_1, and therefore Δ, to vary rather smoothly with frequency. This means that not only is the absolute magnitude of ϵ_2 highly dependent on β, but that any structure in ϵ_2 as a function of frequency will appear almost exclusively in β. This is brought out very clearly by dividing Eqs. (5) and (6) to obtain

$$\epsilon_2\simeq(4\beta/\sin\Delta)(\sin^2\varphi-\epsilon_1). \tag{7}$$

Obviously, great care must be taken in the measurement of β in order to obtain reliable results. We now outline the measures adopted in the present work to overcome this problem.

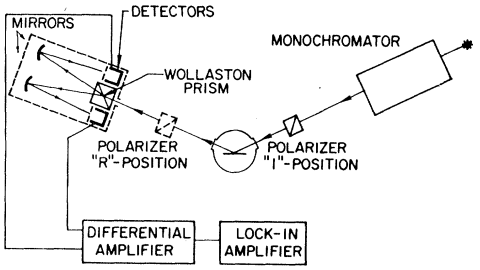

FIG. 1. Diagram of the split-beam ellipsometer. The detectors, mirrors, and Wollaston prism (i.e., the optical components within the broken line) are rigidly mounted on a graduated circle. This detector assembly can be rotated about an axis colinear with the incoming beam.

B. Split-Beam Ellipsometer

The ellipsometer used in these experiments was based on the design of Archard, Clegg, and Taylor,[25] and is illustrated schematically in Fig. 1. The light reflected from the sample is passed into a Wollaston prism which splits the incoming beam into two linearly polarized beams, whose electric vectors are 90° apart. The two beams are picked up by separate detectors. The two detector signals are then subtracted by means of a differential amplifier, and the output is then examined by a lock-in amplifier, which derives its reference from a chopper in front of the light source. A null output is, therefore, obtained whenever the two signals are equal. The novel feature of the present method is the procedure used to deduce ψ and Δ. It consists of observing the changes required in the null settings of a polarizer as it is transferred between the two alternative positions indicated in Fig. 1.

Let us first consider the procedure for determining β (or ψ). The detector-Wollaston assembly, which may be rotated about an axis collinear with an incoming beam, is set so that the detectors "see" the s and p components of polarization. The polarizer is placed in the reflected beam (R position) and set so that its transmitted electric vector is at 45° to the plane of incidence as shown in Fig. 2(a). In this situation, the s and p components entering the Wollaston prism,

[24] M. Born and E. Wolf, in *Principles of Optics* (Pergamon Press, Inc., Great Britain, 1959), p. 617.

[25] J. F. Archard, P. L. Clegg, and A. M. Taylor, Proc. Phys. Soc. (London) **65B**, 758 (1952).

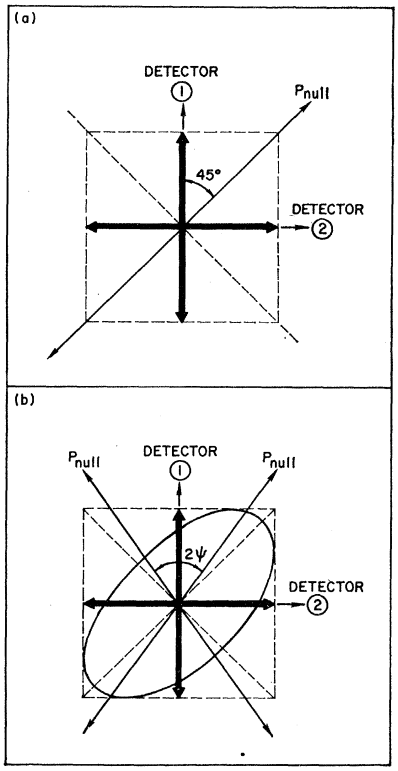

FIG. 2. Geometry of the null settings in the determination of ψ. The bold double-ended arrows represent the peak-to-peak amplitudes of the light "seen" by each detector: (a) polarizer in R position (light entering detector assembly is linearly polarized), (b) polarizer in I position (light entering detector assembly is elliptically polarized).

represented by the bold double-ended arrows in Fig. 2(a), are necessarily equal. The gains of the detectors are then adjusted until a null output is obtained. This operation is necessary in order to compensate any differences in transmission factors, detector sensitivities, etc. The polarizer is then transferred to the incident beam (I position) where we now have to take into account the difference between r_p and r_s. If P denotes the angle made by the polarizer with the plane of incidence, the amplitudes of the two components after reflection are in the proportions $r_p \cos P$ and $r_s \sin P$. Equating these two, we obtain the new null condition

$$P_{\text{null}} = \arctan(r_p/r_s) = \pm\psi. \tag{8}$$

In other words, we may restore the null condition by a slight rotation of the polarizer, the angle of rotation being just β, the quantity of greatest interest. It was found that systematic errors could occur in the null settings, but that the difference between the R-position and I-position null settings tended to remain unaffected. The differential nature of the detector system is particularly advantageous for obtaining reliable values of β.

Let us now consider the determination of Δ. The polarizer is kept in the I position and set at the angle $P = +\psi$ found from the previous operation. We know that in this situation, the s and p components after reflection are equal and that the axes of the ellipse must be oriented at 45° to the plane of incidence, as shown in Fig. 2(b). The procedure is then to rotate the entire detector-Wollaston assembly through 45° so that the Wollaston now resolves the ellipse along its major and minor axes. The peak-to-peak amplitudes of the light "seen" by the detectors are represented by the bold double-ended arrows in Fig. 3(a). The two detector signals will not in general be equal so that the detector system goes off null. The null is restored by reducing the gain of the major axis detector. The polarizer is then returned to the reflected beam (R position), where it once again delivers a linearly polarized beam to the detector system. We have just arranged that a null will be obtained when the detectors see signals in the proportions represented by the bold double-ended arrows shown in Figs. 3(a) and 3(b). Clearly, we can deliver a linearly polarized beam to the detector system which satisfies the same null condition by setting the polarizer at either of the two positions shown in Fig. 3(b). It is easy to show that the angle between these two positions is Δ.

This method does not require a quarter-wave plate or compensator, nor is it necessary to measure any actual intensities or detector signals. Both β and Δ may be read off very directly as differences between appropriate null settings of the polarizer. There are several other sets of settings which are equivalent by symmetry to those described above. For example, a rotation of the entire detector-Wollaston assembly through 90° merely interchanges the detectors. In practice, all equivalent readings were taken and averaged.

The angle of incidence used in all these experiments was 75°. The optical components in the incident and reflected beams were mounted on separate optical benches set 150° apart. The transfer of the polarizer between the I and R positions was accomplished by moving it manually from one bench to the other. Photomultipliers were used as the detectors in the visible and ultraviolet, and lead sulfide cells were used in the infrared. There was an overlap region of wavelengths where both kinds of detector could be operated, and it was always found that agreement was excellent. Since the sensitivity of the detectors varies over their aperture, care was taken always to illuminate the same spot. The concave mirrors shown in Fig. 1 were found useful in this respect. They were arranged so that the detectors were optically conjugate with the point in the Wollaston prism from which the two beams diverged. This ensured that the beams landed always on the same parts of the detectors, and helped to eliminate deviation effects due to any noncollinearity between the incoming beam and the rotation axis of the detector assembly, or to any wavelength dependence of the Wollaston's divergence angle. The photomultipliers and lead sulfide cells were fixed in position side by side,

and the changeover was accomplished by tilting the mirrors to redirect the beams onto the other detectors.

The light entered and left the vacuum chamber in which the samples were prepared through windows of good quality fused quartz. Precautions were taken to ensure that no spurious polarization was introduced into the beam by strain birefringence, often a source of serious error. Several windows were tested by inserting them into the ellipsometer beam and observing any change required in the null settings. The two windows finally chosen showed no appreciable strain birefringence. They were then sealed onto silver gaskets and tested again. They were then tested again while in position on an evacuated chamber to ensure that the pressure differential caused no appreciable strain. We were then confident that the windows introduced no error.

C. Sample Preparation and Experimental Procedure

The specimens used in these experiments were thick opaque films prepared by evaporation in ultra-high vacuum. Samples of 99.99% purity were obtained already sealed under vacuum in glass ampules.[26] The procedure was to first pump and bake out the vacuum chamber with the ampules intact. On cooling to room temperature, pressures low on the 10^{-11}-Torr scale were obtained as a matter of routine. The pump we employed was a Varian Noble Vac-ion 140-liter/sec combination pump. The ampules were then broken open and the subsequent burst of gas pumped away. Pressures on the 10^{-11}-Torr scale could be regained by the following day. The evaporations were performed by heating the ampules from outside the chamber and took from 1 to 2 h. The evaporations onto the multiple-reflection prisms required the longest time, since these prisms subtended quite a large angle at the evaporation source. The pressure rose gradually to $\sim 5\times 10^{-9}$ Torr during the Na evaporations and to $\sim 2\times 10^{-8}$ Torr during the K evaporations. These pressures were measured by an ionization gauge out of line of sight of the source. It is thought that these pressures are due principally to the alkali vapor. The ellipsometric parameter ψ was monitored during the evaporation, and this provided us with an indication of when sufficient material had been deposited. In the early stages of the evaporation, ψ exhibited pronounced oscillations because of interference effects arising from multiple reflections between the front and back surfaces of the film. The evaporation was continued until well after these oscillations had died away and until there was no further change in ψ or Δ on adding more material.

Experiments were performed on the three kinds of samples illustrated in Fig. 4. Free-surface samples were prepared by evaporating the Na or K onto a polished copper substrate shown in Fig. 4(a). It was found necessary to cool the substrate to liquid-nitrogen temperature in order to obtain good specularly reflecting surfaces. Figure 4(b) shows an alternative arrangement in which the light was reflected internally from the back face of a fused-quartz prism. The alkali metal was then evaporated onto this face and the optical constants measured at the quartz-metal interface. This technique was taken a step further by using the multiple-reflection arrangement shown in Fig. 4(c). The alkali-metal sample was evaporated onto either one or both sides of

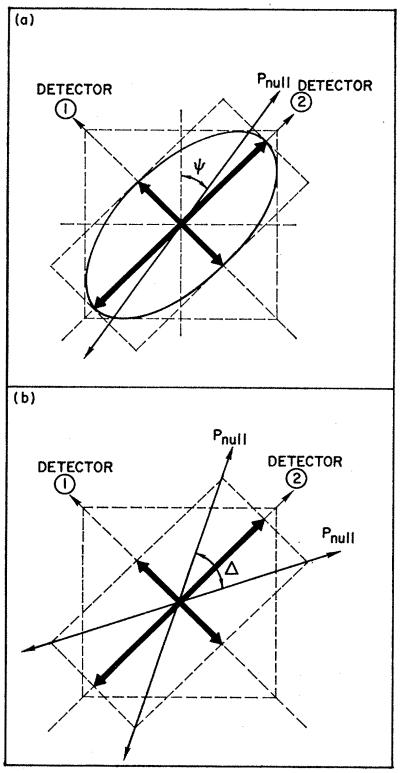

FIG. 3. Geometry of the null settings in the determination of Δ. The bold double-ended arrows represent the peak-to-peak amplitudes of the light "seen" by each detector: (a) polarizer in I position (light entering detector assembly is elliptically polarized), (b) polarizer in R position (light entering detector assembly is linearly polarized).

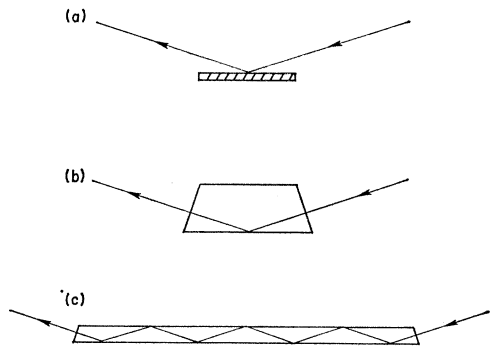

FIG. 4. Three kinds of sample: (a) free surface, (b) single reflection at metal-fused quartz interface, (c) multiple reflections at metal-fused quartz interfaces.

[26] Supplied by Atomergic Chemetals Co., Cerle Place, L. I., N. Y.

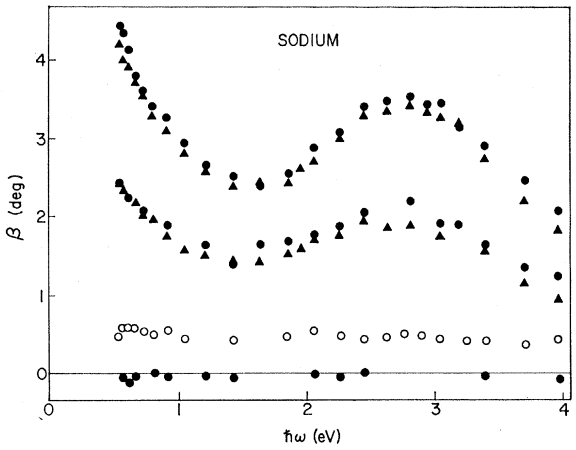

FIG. 5. Raw data for β in sodium. The full circles and triangles refer to measurements of 4β and 7β in separate multiple-reflection experiments. The open circles are measurements of β in a single-reflection experiment. The lowest full circles were obtained in a multiple-reflection experiment prior to evaporation of the sample.

this long fused-quartz plate. The cumulative effect of the seven reflections means, when both sides are covered, that the ellipsometer measures not $\tan\psi e^{i\Delta}$ but $(\tan\psi)^7 e^{i7\Delta}$. This is particularly useful when $\tan\psi$ is close to unity.

When the light is incident on the metal from a dielectric medium, it is necessary to make an allowance for its refractive properties. This is done simply by replacing ϵ_1 and ϵ_2 in Eqs. (2)–(6) by ϵ_1/n_q^2 and ϵ_2/n_q^2, where n_q is the refractive index of the dielectric medium, in our case fused quartz. The faces through which the light enters and leaves the prism were cut normal to the beam, so that they introduced no polarization. One advantage of the prism experiments is that, prior to evaporation, the reflection is total, and $\psi=\frac{1}{4}\pi$ and $\beta=0$. Δ may also be calculated from the known values of n_q and φ, and we, therefore, used these theoretical values of ψ and Δ to test the reliability of the prisms. The condition $\beta=0$ was satisfied accurately by all the prisms. The multiple-reflection prisms, which were made of stock Suprasil, satisfied the Δ condition quite well, but the single-reflection prisms, which were made of specially selected Dynasil, gave Δ values which were slightly low. Less confidence has, therefore, been attached to the results obtained with the single-reflection experiments. A further advantage of the prism-type experiments is that once the sample has been evaporated, the metal-quartz interface is no longer exposed to attack, so that surface contamination problems should be less severe.

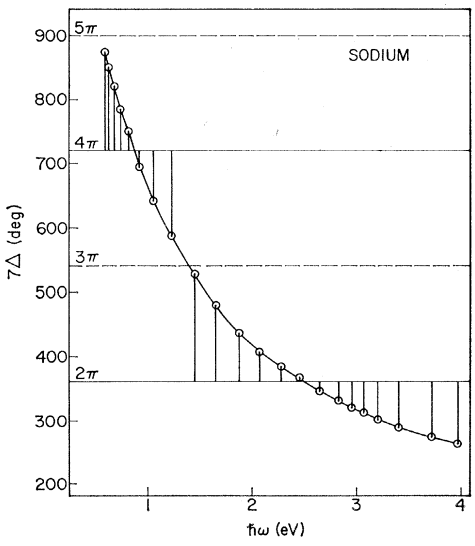

FIG. 6. Values of 7Δ obtained in a multiple-reflection experiment on Na. The vertical lines represent the angles actually measured.

The greatest advantage, however, of the multiple-reflection experiments is the increased accuracy with which the crucial quantity β can be determined. Figure 5 shows the raw data obtained in some typical runs. First of all, β was measured for total reflection before evaporation, then for four metal-quartz reflections (after evaporation on one side of the prism), and then for seven metal-quartz reflections (after evaporation on both sides). Since β may be treated in the small angle approximation, we expect the apparent β measured by the ellipsometer in the single-reflection, four-reflection, and seven-reflection experiments to equal β, 4β, and 7β, respectively. The actual results shown in Fig. 5 do indeed scale in these proportions. This internal consistency inspires further confidence in the reliability of the results. The structure clearly observable in the values of 4β and 7β as a function of frequency, will come through directly in ϵ_2, and will be shown below to be due to interband transitions. The values obtained for β in the free-surface experiments were also consistent with those in the multiple-reflection experiments. The accuracy to which β could be determined counting both instrumental precision and reproducibility was better than 0.02°. β itself varied between 0.2° and 0.6°. A typical value for the error contributed to ϵ_2 would, therefore, be 5%.

In the seven-reflection experiments, the total differential phase change is 7Δ, which may span several multiples of 2π. The measured values of Δ, however, all lie in the range $0\leq\Delta_{\text{meas}}\leq\pi$. The sign of Δ_{meas} is also indeterminate in the ellipsometric technique used here. We, therefore, have

$$\Delta=2\pi n\pm\Delta_{\text{meas}}, \tag{9}$$

where the integer n and the sign of Δ_{meas} have to be determined by other means. The experiments with the single-reflection prisms came in useful here since they provided a prior estimate of Δ and led to a unique assignment. The problem is illustrated further in Fig. 6, where we show the values obtained for 7Δ in Na. The lengths of the vertical lines represent the angles actually measured.

Two of the multiple reflection experiments were performed on both Na and K. Each new experiment employed a new prism. In the first experiment on Na, only β measurements were obtained, since an experimental failure occurred before the Δ measurements could be taken. In this one case, ϵ_2 was calculated using Δ values taken from a free-surface experiment and appropriately modified to allow for the refractive index of fused quartz.

All the measurements described here were performed at room temperature. Measurements of β have been made at lower temperatures by cooling the multiple reflection prisms with liquid nitrogen. However, severe asymmetries were observed in the null settings which we attribute to strain birefringence caused by temperature gradients or contraction of the holder. Therefore, we do not regard these measurements as sufficiently trustworthy for publication at this time.

III. RESULTS AND DISCUSSION

A. Optical Conductivity

Using the accurate values of ψ obtained in the multiple-reflection experiments together with the associated values of Δ, the values of ϵ_2 were calculated and then converted to the optical conductivity according to the definition

$$\sigma(\omega)=\omega\epsilon_2/4\pi. \tag{10}$$

The results are shown for Na and K in Figs. 7 and 8. The closeness of the two sets of measurements presented for each metal demonstrates the good reproducibility which was obtained. $\sigma(\omega)$ is found to fall monotonically with frequency below 1.9 eV in Na and 1.3 eV in K. Above these frequencies, we observe structure which can be readily attributed to conventional interband transitions, as may be seen by comparison with the theoretical curves also shown in Figs. 7 and 8. We now examine, in greater detail, the extent to which the results can be reconciled with theoretical predictions based on the nearly free-electron model.

According to simple theory, we may express the optical conductivity as the sum of a Drude term $\sigma_D(\omega)$ and an interband term:

$$\sigma(\omega)=\sigma_D(\omega)+\sigma_i(\omega). \tag{11}$$

Below the interband threshold, we need consider only the Drude term which may be expressed as

$$\sigma_D(\omega)=Ne^2/m^*\omega^2\tau, \tag{12}$$

where N, τ, and m^* are, respectively, the density of conduction electrons, the relaxation time, and an effective mass. The values of $\sigma_D(\omega)$ shown in Figs. 7 and 8 were calculated from Eq. (12) by taking m^* equal to $1.13m$ for Na and $1.16m$ for K; these values were deduced from the experimental behavior of ϵ_1 as described below. The relaxation time τ was deduced from the known dc conductivity by means of the relation $\sigma_0=Ne^2\tau/m^*$. The experimental values of $\sigma(\omega)$ are seen to be significantly greater than simple theory would suggest. This will be analyzed in more detail below.

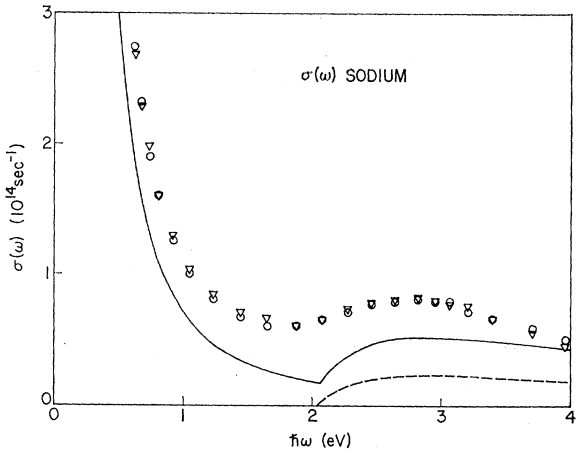

FIG. 7. Optical conductivity of sodium at room temperature: Experimental points are compared with theory. The full curve is the sum of a simple Drude term and Animalu's estimate of the interband absorption. The broken curve was obtained from the Wilson-Butcher expression with $|V_{110}|=0.23$ eV.

Wilson[27] and Butcher[4] have shown that the interband contribution associated with the 110 reciprocal lattice vectors is given by

$$\sigma_i(\omega)=\frac{me^2}{\pi\hbar^4}\frac{|V_{110}|^2}{G_{110}}\frac{(\omega_{\rm hi}-\omega)(\omega-\omega_{\rm lo})}{\omega^3},\quad(\omega_{\rm lo}<\omega<\omega_{\rm hi})$$
$$=0,\quad(\omega>\omega_{\rm hi}\text{ and }\omega<\omega_{\rm lo}) \tag{13}$$

where G_{110} is a reciprocal lattice vector ($G_{110}=2\pi\sqrt{2}/a$,

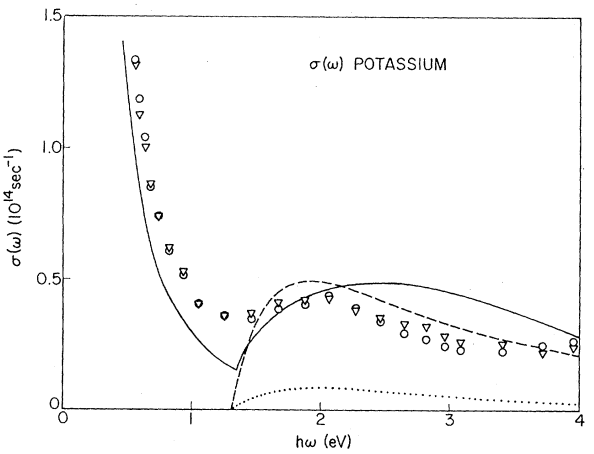

FIG. 8. Optical conductivity of potassium at room temperature: Experimental points are compared with theory. The full curve is the sum of a simple Drude term and Animalu's estimate of the interband absorption. The broken and dotted curves were obtained from the Wilson-Butcher expression with $|V_{110}|=0.24$ eV and $|V_{110}|=0.10$ eV, respectively.

[27] A. H. Wilson, in *The Theory of Metals* (Cambridge University Press, New York, 1936), p. 133.

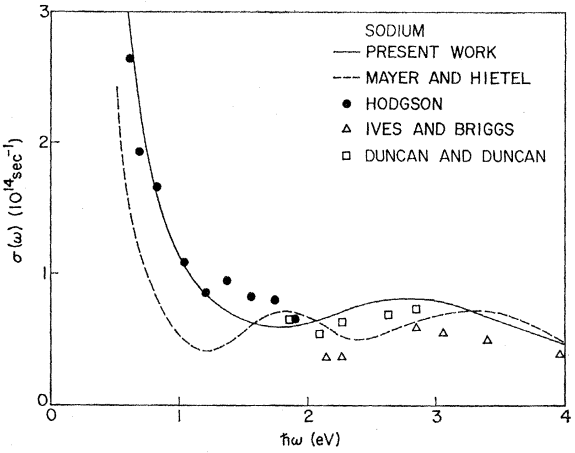

FIG. 9. Optical conductivity of sodium: comparison with results of previous workers.

where a is the lattice constant) and V_{110} is the corresponding Fourier component of pseudopotential. ω_{lo} and ω_{hi} are low and high threshold frequencies given by

$$\hbar\omega_{lo}=(\hbar^2/2m)(G_{110}-2k_F)G_{110}, \quad (14)$$

$$\hbar\omega_{hi}=(\hbar^2/2m)(G_{110}+2k_F)G_{110}. \quad (15)$$

k_F is the free-electron Fermi radius [$=(3\pi^2N)^{1/3}$]. For Na, $\hbar\omega_{lo}=2.0$ eV and for K, $\hbar\omega_{lo}=1.3$ eV. Animalu[28] has extended this nearly free-electron theory to take into account the orthogonalization terms which appear in the true wave functions and which affect the optical matrix elements. He finds that V_{110} in Eq. (13) must be replaced by an "optical pseudopotential," which may differ quite appreciably from V_{110} and which is generally frequency-dependent. His calculated values for $\sigma_i(\omega)$ are shown in Figs. 7 and 8. Also shown in Figs. 7 and 8 are various alternative curves for $\sigma_i(\omega)$ calculated by substituting constant values for V_{110} in Eq. (13). In Fig. 7, the broken curve shows $\sigma_i(\omega)$ for

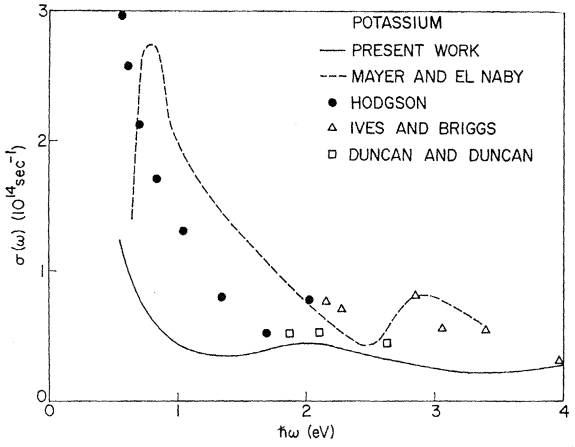

FIG. 10. Optical conductivity of potassium: comparison with results of previous workers.

[28] A. O. E. Animalu, Phys. Rev. **163**, 557 (1967).

Na calculated by putting $V_{110}=0.23$ eV, the value obtained by Lee[29] from de Haas–van Alphen studies. The amplitude of the structure in the observed $\sigma(\omega)$ favors Animalu's calculation. In Fig. 8, the broken curve is $\sigma_i(\omega)$ for K calculated with $V_{110}=-0.24$ eV, the value deduced from Ham's[30] band calculation. The dotted curve was obtained by putting $V_{110}=+0.10$ eV, the model potential value obtained by Animalu and Heine[31] (and tabulated by Harrison[32]). The small amplitude of the structure in the experimental $\sigma(\omega)$ for K seems to be more consistent with the lower value for $|V_{110}|$. However, the interpretation of the data in the interband region is hampered by the largeness of the absorption in the Drude region. Ideally, we would have liked to have fitted Eq. (13) to experiment by using $|V_{110}|$ as an adjustable parameter. But such a procedure will remain unreliable until we know how to subtract out the Drude absorption.

At this point we compare the results of the present work with those of previous workers. Figures 9 and 10 show the present experimental values for $\sigma(\omega)$, now represented as a smooth curve, together with those of Mayer and co-workers,[8,9] Hodgson,[6,7] Ives and Briggs,[1,2] and Duncan and Duncan.[3] Hodgson's results on Na in the infrared agree very well with those of the present work. Duncan and Duncan's results on both Na and K are in reasonable agreement with the present work. Apart from these exceptions, the striking feature is the general lack of agreement. The present measurements, however, are the only ones in which conventional interband transitions can be clearly identified. No evidence has been found for the anomalous peaks observed by Mayer *et al.*, at photon energies below the interband threshold. This discrepancy is perplexing, although it could be due to the fact that the present measurements were made on thick evaporated films, whereas Mayer *et al.* worked with bulk samples. It is conceivable that there is some genuine physical difference between the two kinds of sample. For example, Overhauser[33] has proposed a charge density mechanism for Mayer's optical anomaly, but argues that the effect would be suppressed in film samples because of strain. With this reservation in mind, we will proceed on the assumption that the present results are correct.

Let us now return to the problem of the large absorption below the interband threshold. Several possible explanations come to mind. For example, the film samples used here may have a smaller dc conductivity than bulk material and consequently a smaller τ. Another possibility is the anomalous skin effect, since a quick calculation shows that the mean free path is comparable with the classical skin depth. The anomalous skin effect can be accommodated in Eq. (11)

[29] M. J. G. Lee, Proc. Roy. Soc. (London) **295A**, 440 (1966).
[30] F. S. Ham, Phys. Rev. **128**, 82 (1962).
[31] A. O. E. Animalu and V. Heine, Phil. Mag. **12**, 1249 (1965).
[32] W. A. Harrison, in *Pseudopotentials in the Theory of Metals* (W. A. Benjamin, Inc., New York, 1966), p. 310.
[33] A. W. Overhauser and A. M. de Graaf, Phys. Rev. **168**, 763 (1968).

by writing[34]

$$1/\tau = 1/\tau_b + 1/\tau_s, \tag{16}$$

where $1/\tau_b$ is a bulk scattering frequency to be determined from the dc conductivity $\sigma_0 = Ne^2\tau_b/m^*$. The second term is a surface scattering frequency which, for the case of diffuse scattering of the electrons, has been shown by Holstein[35] and Dingle[36] to be given by

$$1/\tau_s = \tfrac{3}{8}(v_F/c)(4\pi Ne^2/m^*)^{1/2}, \tag{17}$$

where v_F is the Fermi velocity. Using the same values for m^* as before, we find that $1/\tau_s$ is 0.11×10^{14} sec^{-1} for Na and 0.06×10^{14} sec^{-1} for K. These are to be compared with the corresponding values for $1/\tau_b$ which are 0.31×10^{14} sec^{-1} for Na and 0.22×10^{14} sec^{-1} for K. For further comparison, the experimental values of $\sigma(\omega)$ below the interband threshold have been converted to an effective scattering frequency by means of the relation

$$1/\tau_{\text{eff}} = (\omega^2 m^*/Ne^2)[\sigma(\omega)]_{\text{expt}}, \tag{18}$$

which is plotted against the normalized frequency $(\omega/\omega_{\text{lo}})$ in Fig. 11. The theoretical value for $(1/\tau_b + 1/\tau_s)$ agrees well with $1/\tau_{\text{eff}}$ at low frequencies; but this agreement may be fortuitous, since it hinges to a certain extent on the choice of m^*, which was taken throughout to be $1.13m$ for Na and $1.16m$ for K. What does seem clear is that the anomalous skin effect is unable to explain the substantial rise in $1/\tau_{\text{eff}}$ on approaching the interband threshold.[37] Even after inclusion of the anomalous skin effect, or adjustment of the constant τ_b, the theoretical $\sigma(\omega)$ is still expected to fall off as ω^{-2}, while Fig. 11 demonstrates that the fall off is less rapid. We note that the rise of $1/\tau_{\text{eff}}$ with frequency is not confined to Na and K but has also been observed in Cu, Ag,[38] Al,[39] and Li,[40] and therefore, may be an effect of some generality. Gurzhi[41] has shown that the scattering frequency $1/\tau$ should contain an additional term due to electron-electron collisions, which varies as ω^2. Yet another possible explanation of the excess absorption below the interband threshold has been provided in a paper by Nettel.[18] He shows that in addition to simple phonon-aided transitions, there are other phonon-aided processes which involves a virtual interband transition as an intermediate stage. The perturbation-theory energy denominator associated with this interband part of the transition diminishes as the threshold is approached causing a corresponding increase in importance of these extra processes. Numerical calculations for Na at room temperature[42] indicate that this extra contribution to $\sigma(\omega)$ would be about 0.1×10^{14} sec^{-1} at 0.6 eV and would rise steadily to

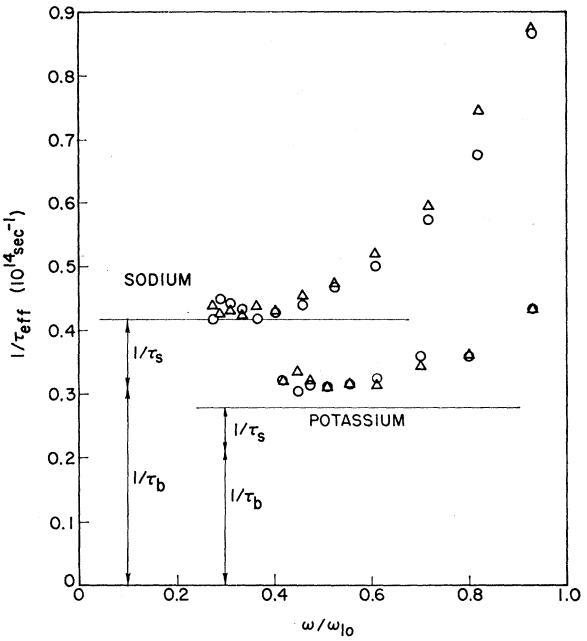

FIG. 11. The effective scattering time, $1/\tau_{\text{eff}} \equiv (\omega^2 m^*/Ne^2) \times[\sigma(\omega)]_{\text{expt}}$, for both Na and K below the interband threshold.

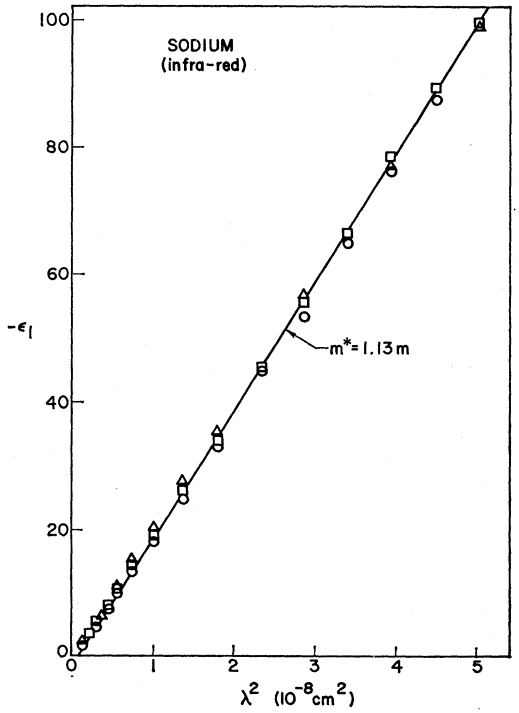

FIG. 12. Real part of the dielectric constant for sodium in the infrared. The open circles refer to a multiple reflection experiment at metal-fused quartz interfaces. The squares and triangles refer to separate free-surface experiments.

[34] The treatment here follows closely that of Hodgson in Ref. 6.
[35] T. Holstein, Phys. Rev. **88**, 1427 (1952).
[36] R. B. Dingle, Physica **19**, 729 (1953); the relevant equation is number (9.23).
[37] We should add the reservation that Eq. (17) was derived for normal incidence. At oblique incidence, as was used here, Kliewer and Fuchs (Ref. 20) have shown that the situation is more complicated and that Eqs. (2) and (3) may also break down.
[38] H. Ehrenreich and H. R. Phillip, Phys. Rev. **128**, 1622 (1962).
[39] H. Ehrenreich, H. R. Phillip, and B. Segall, Phys. Rev. **132**, 1918 (1963).
[40] J. N. Hodgson, Ref. 9, p. 60.
[41] R. N. Gurzhi, Zh. Eksperim. i Teor. Fiz. **35**, 965 (1958) [English transl.: Soviet Phys.—JETP **8**, 673 (1959)].
[42] At this point we interpolated between Nettel's values at −78 and 100°C.

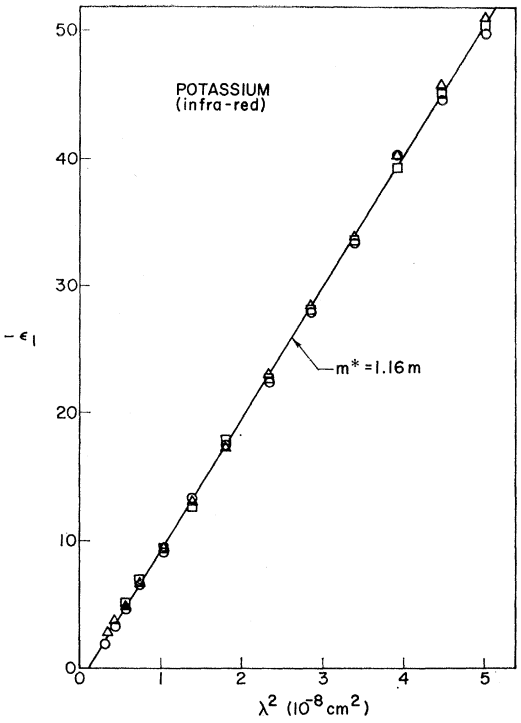

FIG. 13. Real part of the dielectric constant for potassium in the infrared. The triangles refer to a free-surface experiment. The circles and squares refer to two separate multiple-reflection experiments at metal-fused quartz interfaces.

0.4×10^{14} sec^{-1} at 1.8 eV. A glance at Fig. 7 reveals that a contribution of just this magnitude would remedy the discrepancy between theory and experiment. Further calculations along these lines would seem to be welcome.

B. ε_1 and the Optical Mass

The real part of the dielectric constant, ϵ_1, may also be expressed as the sum of several terms[5]

$$\epsilon_1=1+4\pi N\alpha_0-Ne^2\lambda^2/m^*\pi c^2+\epsilon_{1i}. \qquad (19)$$

The $4\pi N\alpha_0$ term arises from the polarizability of the ion cores; the third term is due to the response of the conduction electrons and involves λ, the free-space wavelength of the light; and the fourth term ϵ_{1i} is due to interband transitions. For frequencies well below the interband threshold, ϵ_{1i} is a constant, and we expect ϵ_1 to vary linearly with λ^2, the slope yielding a value for m^*. The infrared data for $-\epsilon_1$ obtained in a number of experiments is plotted against λ^2 in Figs. 12 and 13. Linear relationships were indeed observed and the values found for m^* were $1.13m$ for Na and $1.16m$ for K. The slopes determined from the fitting procedure had a standard deviation of about 1%. However, the actual limits of error are somwhat larger than this, since reference to Eq. (2) shows that an error in the determination of the angle of incidence φ could cause an appreciable systematic error. The total uncertainty in the quoted values for m^* from all sources is estimated to be $\pm2\%$. Particularly encouraging is the good agreement obtained between the experiments performed at free surfaces and those performed at quartz-metal interfaces.

As the frequency approaches the interband threshold ω_{1o}, we may no longer treat ϵ_{1i} as a constant and we expect departures from the linear relationship. The experimental results for $-\epsilon_1$ in the visible and ultraviolet regions of the spectrum are shown in Figs. 14 and 15. Also shown in each figure is the continuation of the line obtained by fitting the infrared data. In spite of the increased scatter of the data in this region, significant departures from this line can be discerned. Cohen has shown[5] that in certain circumstances ϵ_{1i} can be expressed as the sum of two terms one of which is constant and the other of which varies as λ^2. The term which goes as λ^2 can then be absorbed into the third term of Eq. (19) by replacing m^* by what Cohen calls an "optical mass" $m_{\rm opt}$. In fact, whenever a linear relationship is observed between ϵ_1 and λ^2, this serves to define an appropriate optical mass. It was found in all experiments on both metals that $-\epsilon_1$ returned to a steeper linear variation with λ^2 at the shorter wavelengths. Fitting new straight lines to the data below about $\lambda=0.5\ \mu$ gave $m_{\rm opt}=1.07m$ for Na and $m_{\rm opt}=1.06m$ for K. The lines are shown in Figs. 14 and 15. Extrapolating these lines, we find that the intercept on the ordinate occurs at $\epsilon_1=1.0$ in Na and at $\epsilon_1=1.2$ in K. The plasma frequency was also determined from the wavelength at which $\epsilon_1=0$, and was found to be 5.65 ± 0.1 eV in Na and 3.8 ± 0.1 eV in

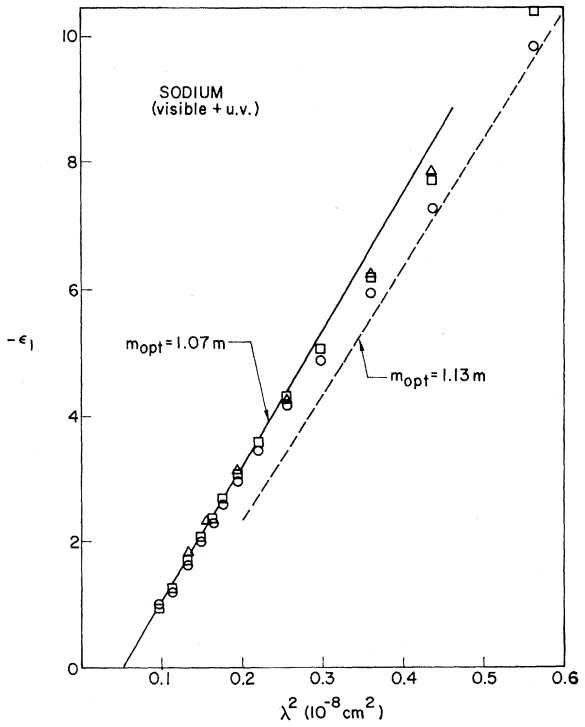

FIG. 14. Real part of the dielectric constant for sodium in the visible and near ultraviolet. The circles, squares, and triangles refer to the same experiments as in Fig. 12.

TABLE I. Values for m_{opt}/m and m^*/m obtained in different frequency regions.

Source	Na	K
Vacuum ultraviolet		
Sutherland *et al.*	1.06	1.06
Visible and near ultraviolet		
Present work	**1.07**	**1.06**
Hodgson	1.00	...
Mayer *et al.*	1.17	1.00
Cohen's analysis of Ives and Briggs's data	1.01	1.08
Near infrared		
Present work	**1.13**	**1.16**
Hodgson	1.08	1.18
Mayer *et al.*	1.27	1.00(1.16)[a]
Far infrared		
Althoff and Hertz	1.00	1.17
Microwave		
Cyclotron mass obtained by Grimes and Kip[b]	1.24	1.21

[a] An amended value from an alternative analysis by Hodgson (Ref. 7).
[b] C. C. Grimes and A. F. Kip, Phys. Rev. **132**, 1991 (1963).

K. Our data in this region match quite well with the vacuum ultraviolet data of Sutherland and coworkers,[11,12] who found that m_{opt} was equal to $1.06m$ for both metals.

In Table I, we collect the values of m_{opt} obtained by different workers in various frequency ranges. The scatter of the different estimates is least severe in the case of potassium, and we are able to observe a decreasing trend in the experimental values for the mass as we proceed to higher frequencies. It is believed that there are two contributing factors to this effect. First, at low

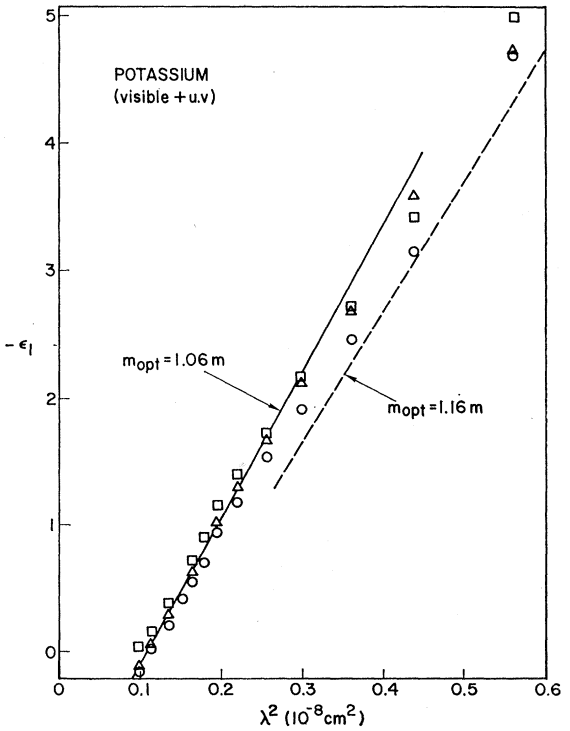

FIG. 15. Real part of the dielectric constant for potassium in the visible and near ultravoilet. The circles, squares, and triangles refer to the same experiments as in Fig. 13.

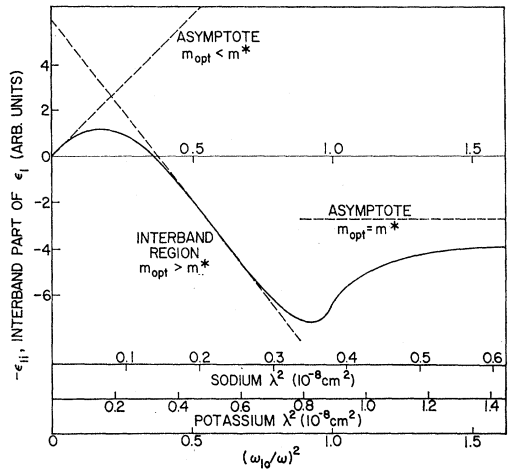

FIG. 16. Negative of ϵ_{1i}, the interband contribution to ϵ_1, the real part of the dielectric constant, according to the nearly free-electron theory. A linear dependence on λ^2 can be found in the three separate regions shown.

frequencies the mass is enhanced by electron-electron and by electron-phonon interactions. This dressing effect is expected to become less important with increasing frequency. Second, there are band structure effects (i.e., optical mass effects due to ϵ_{1i}). The values of m_{opt} for sodium show much more scatter although it is still possible to discern the decreasing trend with increasing frequency. For example, although the author, Hodgson, and Mayer and Hietel obtained different values for m_{opt}, the difference is systematic. On going from the near infrared to the near ultraviolet (i.e., on crossing the interband threshold), each set of data shows a decrease in m_{opt} of 6–8%. Cohen[5] has predicted a change of this sense, but we should treat this agreement with caution, since it is shown below that his argument may not be complete.

TABLE II. Averaged optical constants of sodium.

$\hbar\omega$ (eV)	ϵ_1	ϵ_2	$\sigma(\omega)$ (10^{14} sec^{-1})	R
0.554	−99.28	5.231	3.503	0.9896
0.585	−89.27	4.553	3.220	0.9893
0.626	−77.40	3.637	2.752	0.9895
0.674	−65.49	2.835	2.310	0.9895
0.734	−55.03	2.184	1.938	0.9895
0.810	−44.45	1.638	1.604	0.9892
0.922	−33.89	1.148	1.280	0.9887
1.055	−26.12	0.797	1.016	0.9885
1.228	−18.94	0.558	0.828	0.9872
1.442	−13.87	0.395	0.689	0.9858
1.653	−10.36	0.319	0.637	0.9827
1.873	− 7.623	0.268	0.607	0.9777
2.067	− 6.144	0.261	0.653	0.9709
2.271	− 4.986	0.262	0.718	0.9616
2.455	− 4.275	0.260	0.773	0.9534
2.638	− 3.538	0.249	0.794	0.9434
2.818	− 3.082	0.240	0.818	0.9353
2.952	− 2.656	0.221	0.788	0.9287
3.064	− 2.358	0.212	0.786	0.9212
3.204	− 2.169	0.192	0.743	0.9213
3.397	− 1.755	0.162	0.664	0.9154
3.711	− 1.278	0.125	0.560	0.9078
3.967	− 1.010	0.099	0.477	0.9064

TABLE III. Averaged optical constants of potassium.

$\hbar\omega$ (eV)	ϵ_1	ϵ_2	$\sigma(\omega)$ (10^{14} sec^{-1})	R
0.554	−50.34	1.968	1.318	0.9892
0.585	−45.19	1.596	1.129	0.9897
0.626	−39.93	1.343	1.016	0.9896
0.674	−33.53	1.054	0.859	0.9895
0.734	−28.11	0.833	0.739	0.9892
0.810	−22.57	0.625	0.612	0.9889
0.922	−17.53	0.468	0.522	0.9880
1.055	−12.78	0.318	0.405	0.9871
1.228	− 9.22	0.243	0.360	0.9844
1.442	− 6.54	0.205	0.358	0.9789
1.653	− 4.81	0.194	0.388	0.9700
1.873	− 3.38	0.184	0.416	0.9554
2.067	− 2.62	0.172	0.431	0.9429
2.271	− 2.05	0.141	0.387	0.9375
2.455	− 1.637	0.117	0.348	0.9329
2.638	− 1.296	0.097	0.309	0.9286
2.818	− 1.040	0.087	0.295	0.9202
2.952	− 0.804	0.074	0.265	0.9124
3.064	− 0.637	0.065	0.242	0.9050
3.397	− 0.299	0.057	0.234	0.8526
3.711	− 0.075	0.051	0.231	0.7184
3.967	0.074	0.052	0.249	0.3107

It is of interest to investigate the extent to which the observed changes in $m_{\rm opt}$ can be attributed to the interband transitions which we have observed in $\sigma(\omega)$. In the nearly free-electron model, it may be shown, either from first principles[27] or by a Kramers-Krönig inversion of Eq. (13), that the interband contribution to ϵ_1 associated with the 110 reciprocal lattice vectors is given by

$$\epsilon_{1i}(\omega)=\frac{8me^2|V_{110}|^2}{\pi\hbar^4 G_{110}\omega^4}\Bigg[\omega^2\left\{\ln\frac{\omega_{\rm hi}}{\omega_{\rm lo}}-\frac{\omega_{\rm hi}^2-\omega_{\rm lo}^2}{2\omega_{\rm hi}\omega_{\rm lo}}\right\}+\omega_{\rm lo}\omega_{\rm hi}\ln\frac{\omega_{\rm hi}}{\omega_{\rm lo}}-\tfrac{1}{2}(\omega_{\rm lo}-\omega)(\omega_{\rm hi}-\omega)\ln\left|\frac{\omega_{\rm hi}-\omega}{\omega_{\rm lo}-\omega}\right|-\tfrac{1}{2}(\omega_{\rm lo}+\omega)(\omega_{\rm hi}+\omega)\ln\left(\frac{\omega_{\rm hi}+\omega}{\omega_{\rm lo}+\omega}\right)\Bigg]. \quad (20)$$

The variation of $-\epsilon_{1i}$ is plotted against the normalized quantity $(\omega_{\rm lo}/\omega)^2$ in Fig. 16. Since $\omega_{\rm lo}$ and $\omega_{\rm hi}$ scale to the Fermi energy, the form of ϵ_{1i} shown in Fig. 16 applies equally well to all bcc monovalent free-electron metals. The values of λ^2 appropriate to Na and K have been inserted on additional scales to facilitate comparison of Fig. 16 with Figs. 14 and 15. The theoretical ϵ_{1i} shows the characteristic Kramers-Krönig "wiggle," and it is possible to find linear behavior in three regions, thus enabling us to define three separate optical masses. For frequencies well below the interband threshold ϵ_{1i} is constant and $m_{\rm opt}=m^*$. At frequencies above the high-frequency cutoff $\omega_{\rm hi}$, there is an asymptote with a slope having $m_{\rm opt}<m^*$. Within the interband region, we can find an approximate linear behavior for ϵ_{1i} with $m_{\rm opt}>m^*$. Notice that this is the exact opposite of Cohen's prediction.[43]

Comparison of the theoretical ϵ_{1i} shown in Fig. 16 with the experimental results in Figs. 14 and 15 does reveal qualitative agreement. However, we find theoretically that the high-frequency region for which $m_{\rm opt}<m^*$ should occur for $\lambda\lesssim 0.25\,\mu$ in Na and for $\lambda\lesssim 0.35\,\mu$ in K. Yet in both Na and K, linear relationships yielding $m_{\rm opt}<m^*$ were observed experimentally for wavelengths as high as $0.5\,\mu$. We must conclude that Eqs. (13) and (20) are probably inadequate or incomplete as descriptions of the interband contributions to the optical constants. For example, a qualitative consideration of the Kramers-Krönig relations[43] shows that the observation of $m_{\rm opt}<m^*$ at unexpectedly large wavelengths is consistent with the existence of further structure in $\sigma(\omega)$ at frequencies above those accessible in the present work. In this connection, we note that evidence of interband transitions occurring above the plasma frequency has already been found in several alkali metals by Matatagui and Cardona[44] using a modulation technique.

C. Numerical Tabulation

Finally, for the convenience of future workers, our new optical data are presented in numerical form in Tables II and III. This best set was obtained by averaging our values for ϵ_1 and ϵ_2 at each wavelength. The real and imaginary parts of the refractive index were then calculated from them in the usual way

$$(n-ik)=(\epsilon_1-i\epsilon_2)^{1/2}, \quad (21)$$

and the normal reflectivity was also calculated from

$$R=\frac{(n-1)^2+k^2}{(n+1)^2+k^2}. \quad (22)$$

ACKNOWLEDGMENTS

I am deeply grateful to Professor William E. Spicer for suggesting these experiments, for placing the facilities of his laboratory at my disposal, and for his ever friendly advice. Thanks also are due to J. McGowan and S. Wanner for their skilled work in constructing apparatus, to R. Y. Koyama for help in testing the ellipsometer, and to my colleagues at Stanford for stimulating discussions.

[43] Cohen (Ref. 5) envisages a situation in which the frequency ω lies well within an interband region which covers a wide range of frequencies; the interband transition frequencies are denoted by ω_{rc}. The transitions for which $\omega_{rc}\sim\omega$ are then ignored, and Cohen confines his attention to those for which $\omega_{rc}\gg\omega$ and $\omega_{rc}\ll\omega$. In this approximation, ϵ_{1i} then contains a term which goes as $-\omega^{-2}$ leading to $m_{\rm opt}<m^*$. One may arrive at the same conclusion by a qualitative consideration of the Kramers-Krönig relations. If $\sigma_i(\omega)$ can be divided into two well-*isolated* pieces of structure, it is easy to show that in the intermediate frequency region a plot of ϵ_{1i} against ω^{-2} will show a region of negative slope leading to $m_{\rm opt}<m^*$. However, if $\sigma_i(\omega)$ consists of a single broad piece of structure, the Kramers–Krönig relations will give an $\epsilon_{1i}(\omega)$ much like that shown in Fig. 16, having $m_{\rm opt}>m^*$ in the middle of the interband range. The discrepancy in Cohen's argument presumably lies in the neglect of those transitions for which $\omega_{rc}\sim\omega$. Since they contribute terms to ϵ_{1i} of the form $(\omega_{rc}^2-\omega^2)^{-1}$ their omission is suspect.

[44] E. Matatagui and M. Cardona, Solid State Commun. **6**, 313 (1968).